

Surface Characterization and Electrocatalytic Properties of the $\text{Ti}/\text{Ir}_{0.3}\text{Ti}_{(0.7-x)}\text{Pb}_x\text{O}_2$ -Coated Electrodes for Oxygen Evolution Reaction in Acidic Media

Adriana de Oliveira-Sousa and Pedro de Lima-Neto*

Departamento de Química Analítica e Físico-Química, Universidade Federal do Ceará, CP 6035, 60455-900, Fortaleza - CE, Brazil

Neste trabalho é feita uma investigação sistemática de caracterização morfológica e da atividade eletrocatalítica de eletrodos de Ti revestidos com camadas de $\text{Ir}_{0.3}\text{Ti}_{(0.7-x)}\text{Pb}_x\text{O}_2$ ($0 \leq x \leq 0,7$), usando a reação de desprendimento de oxigênio (RDO), em meio de H_2SO_4 $0,5 \text{ mol dm}^{-3}$, como modelo. Os eletrodos foram preparados pela decomposição térmica de IrCl_3 , TiCl_3 e $\text{Pb}(\text{NO}_3)_2$ a 600°C por 1 h usando Ti como suporte. A difração de raios-X mostrou que a camada é cristalina e permitiu identificar a presença dos correspondentes óxidos nas camadas. A caracterização da morfologia superficial das amostras, antes e após uso sob desprendimento de oxigênio (experimento de Tafel), foi feita por microscopia eletrônica de varredura (MEV). As análises das micrografias mostram que a RDO promove a dissolução da camada de óxido, indicando que o mecanismo de desativação destes eletrodos está associado à dissolução da camada. Os voltamogramas cíclicos obtidos em H_2SO_4 $0,5 \text{ mol dm}^{-3}$ a 20 mV s^{-1} , à temperatura ambiente, mostram que o par redox $\text{Ir}^{3+}/\text{Ir}^{4+}$ controla a eletroquímica superficial dos eletrodos. Os valores de carga anódica são relacionados à área ativa dos eletrodos e mostram que esta aumenta com teor de Pb na camada, atingindo um máximo em 50% de Pb. Após a RDO, a área superficial das camadas aumenta. Os valores dos coeficientes de Tafel são independentes do teor de Pb na camada com valores de aproximadamente $60 \text{ mV decade}^{-1}$, sugerindo que somente sítios de Ir são ativos para a RDO. Os valores de corrente normalizadas (i/q_a) mostram alguma inibição da RDO quando TiO_2 é substituído por PbO_2 , sugerindo que esse óxido pode ser uma boa escolha para melhorar a seletividade do sistema. A ordem de reação com relação à concentração de íons H^+ é zero a sobrepotencial e força iônica constantes. Os valores da inclinação de Tafel e ordem de reação indicam que a RDO ocorre por um único mecanismo.

In this work a systematic investigation was carried out of the surface characterization and electrocatalytic activity of $\text{Ti}/\text{Ir}_{0.3}\text{Ti}_{(0.7-x)}\text{Pb}_x\text{O}_2$ -coated electrodes ($0 \leq x \leq 0.7$), using the oxygen evolution reaction (OER) in $0.5 \text{ mol dm}^{-3} \text{H}_2\text{SO}_4$ as model. The electrodes were prepared by thermal decomposition of IrCl_3 , TiCl_3 and $\text{Pb}(\text{NO}_3)_2$ at 600°C for 1 h using Ti as support. X-ray diffraction shows that the layers are crystalline and that the corresponding metal oxides are present. The surface morphology of the samples, before and after use under extensive oxygen evolution (Tafel experiment), was characterized by Scanning Electron Microscopy and the micrograph analyses show that the OER promotes the dissolution of the oxide layer. The redox processes occurring on the surface were characterized by cyclic voltammetry at 20 mV s^{-1} in 0.5 mol dm^{-3} aqueous H_2SO_4 , at room temperature, and were controlled by the $\text{Ir}^{3+}/\text{Ir}^{4+}$ couple. The measured anodic voltammetric charge is related to the active area of the electrode showing that the replacement of TiO_2 by PbO_2 increases the surface area with the higher value being at 50 mol% PbO_2 . After oxygen evolution, the surface area increases slightly. Tafel slopes are independent of Pb content with the values around $60 \text{ mV decade}^{-1}$, which suggest that only Ir sites are active for OER. The values of normalized current (i/q_a) show some inhibition of the OER as TiO_2 is replaced by PbO_2 , suggesting that PbO_2 can be a good choice, with potential to improve the selectivity of the system. The reaction order with respect to H^+ ion is zero at constant overpotential and ionic strength. The values of Tafel slope and reaction order indicate that a single reaction mechanism is operating.

Keywords: oxygen evolution reaction, electrocatalysis, iridium dioxide electrodes, lead oxide

* e-mail: pln@ufc.br

Introduction

Dimensionally Stable Anodes (DSA) are electrode materials widely studied for several electrochemical applications: (a) oxygen and chlorine evolution reactions,¹ (b) electrochemical degradation of organic contaminants in waste water treatment,²⁻⁷ (c) electrosynthesis of organic polymer⁸ and (d) electrowinning of metals.⁹

These kinds of electrode materials are produced by a combination of an active catalyst component (*e. g.* RuO_2 or IrO_2) and a stabilizing component (*e. g.* TiO_2 or Ta_2O_5). RuO_2 -based layers deposited on a titanium substrate are the most traditional electrode material but, in recent years, IrO_2 has been used to substitute RuO_2 as the active electrocatalyst component in the layer composition because it is more resistance to corrosion, while showing only slightly less electrocatalytic activity.¹⁰

A third component can be added to the electrocatalyst layer to modify the electrochemical and electrocatalytic properties of the electrodes. Boodts and Trasatti¹¹⁻¹⁶ have carried out systematic investigations of the physicochemical and electrochemical properties of ternary DSA electrodes using PtO_2 , CeO_2 and SnO_2 as the third component. The methodology used by these authors is to substitute TiO_2 by one of these oxides in the 30 mol % RuO_2 + 70 mol % TiO_2 or 30 mol % IrO_2 + 70 mol % TiO_2 systems.

PbO_2 electrodes are known to be high-overpotential anode materials for oxygen evolution reaction (OER), which permits their use as anodes to solve environmental problems such as the electrochemical incineration of organic contaminants,¹⁷ for the treatment of fluoride-containing electrolytes¹⁸ and for the conversion of Cr^{6+} to Cr^{3+} ions in aqueous solutions.¹⁹ Because of these applications of such oxide layers, it is relevant to study OER, as a model reaction, since the occurrence of this reaction decreases the global efficiency of the reactions of interest.

SnO_2 is the oxide usually added to the MO_2 - TiO_2 ($M = \text{Ru}$ or Ir) layers to enhance selectivity in the process of the electrochemical oxidation of organic compounds or in the chlorine evolution reaction (CLER) because Ti/SnO_2 -coated electrodes present higher efficiency for these reactions than the electrodeposited Ti/PbO_2 -coated electrodes. Additionally, Laurindo *et al.*²⁰ showed that Ti/PbO_2 , produced by the thermal-electrochemical method, presents a much higher overpotential for OER than electrodeposited Ti/PbO_2 -coated electrodes in acid media, but the currents obtained for the thermal-electrochemical Ti/PbO_2 -coated electrodes were quite low. These results indicated that thermal PbO_2 can be a potential candidate to be added as the third component to the IrO_2 - TiO_2 layers to improve the selectivity of the system, associated with a good electrical conductivity of the

IrO_2 -based layers. Thus, the objective of this work is to carry out a systematic investigation of $\text{Ti}/\text{Ir}_{0.3}\text{Ti}_{(0.7-x)}\text{Pb}_x\text{O}_2$ -coated electrodes ($0 \leq x \leq 0.7$) using the oxygen evolution reaction in $0.5 \text{ mol dm}^{-3} \text{ H}_2\text{SO}_4$, as a model reaction, to analyze the influence of the PbO_2 content on the electrocatalytic properties of the electrodes. The electrocatalyst layers obtained were characterized by X-ray diffraction and by scanning electron microscopy before and after extensive oxygen evolution in Tafel experiments.

Experimental

Preparation of the electrodes

Ti-coated electrodes were prepared by thermal decomposition of $\text{IrCl}_3 \cdot 3\text{H}_2\text{O}$ (Fluka), TiCl_3 (Merck) and $\text{Pb}(\text{NO}_3)_2$ (Merck) in an air furnace atmosphere at $600 \text{ }^\circ\text{C}$ with a nominal layer composition of $\text{Ir}_{0.3}\text{Ti}_{(0.7-x)}\text{Pb}_x\text{O}_2$ ($0 < x < 0.7$). The coating solution of the each precursor was prepared by dissolving the salt in 10% (v/v) aqueous HCl to give 0.2 mol dm^{-3} . The precise concentrations were obtained by thermogravimetric analysis. The Ti supports ($10 \times 10 \times 1 \text{ mm}$) were initially sandblasted and etched in boiling 10% aqueous oxalic acid for 5 min to remove surface oxides. The electrocatalyst layers were obtained by applying the coating mixture, in the required mole ratio of the precursors, to both faces of the Ti-support by brushing, followed by evaporation of the solvent using a flux of hot air. The layers were next heated for 5 min in a furnace pre-heated to the desired temperature. This procedure was repeated until the desired oxide loading (in the range of 1.3 mg cm^{-2} - 2.0 mg cm^{-2} , depending on the composition and corresponding to a nominal thickness of about 2 nm) was reached. The layers were finally annealed at the same temperature for 1 h. Duplicate samples of the electrodes were prepared in all cases.

Physical characterization

The structure of the layer and the qualitative identification of the corresponding oxides were carried out by X-ray diffraction analysis using a Siemens Mod. D5000 instrument. The surface morphology of the coatings, before and after Tafel experiments, were examined by Scanning Electron Microscopy (SEM) in a Zeiss DSM 960 microscope at an accelerating voltage of 20 keV.

Electrochemical measurements

In all electrochemical experiments, platinum foils were used as auxiliary electrodes and a hydrogen electrode in

the same solution (RHE) was used as reference. The water was purified by Milli-Q system (Millipore) and the electrolyte (H_2SO_4) was p.a. from Merck (Darmstadt).

The surface redox behaviors of the coatings were characterized in 0.5 mol dm^{-3} aqueous H_2SO_4 solutions at 25°C by cyclic voltammetry at 20 mV s^{-1} , between 0.4 V and 1.4 V (E vs. RHE). The oxygen evolution reaction was studied under potentiostatic control in the same electrolyte. A PAR model 273A potentiostat/galvanostat linked to a PC microcomputer and operated through the M270 EG&G PARC software was used for data acquisition in the cyclic voltammetric and potentiostatic measurements. The order of the reaction with respect to H^+ ion was determined by varying the H_2SO_4 concentration between 0.1 to 1.0 mol dm^{-3} while keeping the ionic strength constant at 1 mol dm^{-3} by addition of Na_2SO_4 . These experiments were carried out applying an electrode potential of 1.5 V and recording the current after 10 min .

Results and Discussion

Physical characterization

Figure 1 shows a typical X-ray diffractogram obtained for the $\text{Ti}/\text{Ir}_{0.3}\text{Ti}_{(0.7-x)}\text{Pb}_x\text{O}_2$ -coated electrodes. The diffractograms revealed characteristic peaks related to the substrate and well defined peaks for the layer, characterizing a crystalline structure. The XRD data for the main peaks observed in the diffractograms were compared with XRD data from JCPDS (Joint Committee of Powder Diffraction Standards). As can be observed from this figure, characteristic peaks corresponding to IrO_2 , TiO_2 and PbO_2 were qualitatively identified. However, it was not possible to correlate the peaks present at diffraction angles $2\theta = 21.6$ and 22.6 with one of those oxides and the peak at diffraction angle $2\theta = 42.9$ is similar to one typical of PbO .

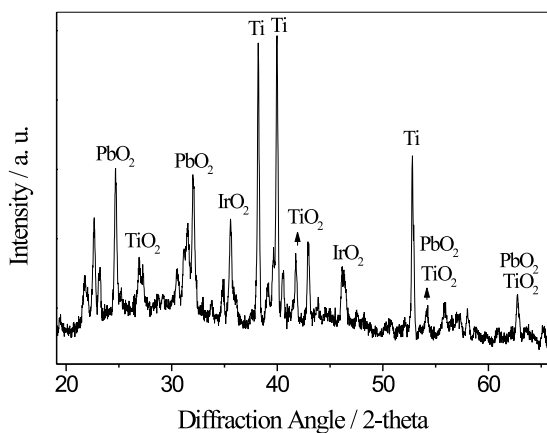


Figure 1. Typical X-ray diffractogram of $\text{Ti}/\text{Ir}_{0.3}\text{Ti}_{(0.7-x)}\text{Pb}_x\text{O}_2$ -coated electrodes

Figure 2 shows the SEM micrographs of $\text{Ir}_{0.3}\text{Ti}_{(0.7-x)}\text{Pb}_x\text{O}_2$ layers, before and after being submitted to extensive oxygen evolution in the Tafel experiments. The micrographs of the fresh layers reveal a typical cracked-mud morphology of the binary $\text{Ir}_{0.3}\text{Ti}_{0.7}\text{O}_2$ sample (Figure 2a), while the replacement of the TiO_2 with PbO_2 produces a coating surface with microcracks on the top for ternary coatings (Figure 2c) and a granular and compact coating surface for the binary $\text{Ir}_{0.3}\text{Pb}_{0.7}\text{O}_2$ layer (Figure 2e). The SEM micrographs of the layers which were submitted to extensive oxygen evolution show that surface morphology changes in all cases. The $\text{Ir}_{0.3}\text{Ti}_{0.7}\text{O}_2$ layer (Figure 2b) micrograph shows the presence of microcrystallites on the plates which is not observed in the fresh sample (Figure 2a). In the ternary layer (Figure 2d), the oxygen evolution promotes a cracked surface, while in binary $\text{Ir}_{0.3}\text{Pb}_{0.7}\text{O}_2$ the presence of microcrystallites in the form of needles can be observed (Figure 2f). The analysis of these micrographs suggests that the OER promotes the dissolution of the oxide layer. These results are in close agreement with those previously obtained for $\text{Ti}/\text{Ru}_x\text{Ir}_{(0.7-x)}\text{O}_2$ -coated and Ti/IrO_2 -coated electrodes, which associate the coating dissolution as one of the possible electrode deactivation process during electrode wear.^{21,22}

Electrochemical measurements

In all the electrochemical experiments, the duplicate samples presented, on average, the same behavior. The cyclic voltammograms of all samples of $\text{Ti}/\text{Ir}_{0.3}\text{Ti}_{(0.7-x)}\text{Pb}_x\text{O}_2$ -coated electrodes in 0.5 mol dm^{-3} H_2SO_4 were similar to the voltammograms shown in Figure 3. These voltammograms show that the ternary coatings (Figure 3b) present higher current density than the binary coatings (Figure 3a and 3c). The increase of the current density is related to the higher surface area of the ternary coatings. The cyclic voltammograms of the binary $\text{Ir}_{0.3}\text{Pb}_{0.7}\text{O}_2$ layer also present current values higher than those observed for the $\text{Ir}_{0.3}\text{Ti}_{0.7}\text{O}_2$ layer. The broad peak observed at 0.85 V has been attributed to the $\text{Ir(III)}/\text{Ir(IV)}$ transition¹² which suggests that the surface electrochemistry is controlled by this redox transition. All these results are similar to those previously reported for $\text{Ti}/\text{Ru}_{0.3}\text{Ti}_{(0.7-x)}\text{Sn}_x\text{O}_2$ -coated¹¹ and $\text{Ti}/\text{Ir}_{0.3}\text{Ti}_{(0.7-x)}\text{Ce}_x\text{O}_2$ -coated¹² electrodes.

The variation of the anodic voltammetric charge density (q_a), obtained from the voltammograms shown in Figure 3, is related to modifications in the surface morphology and the charge is taken as a parameter proportional to the active surface area.²³ The dependence of q_a on the composition of the layer is presented in Figure 4, which reveals that the anodic charge density increases

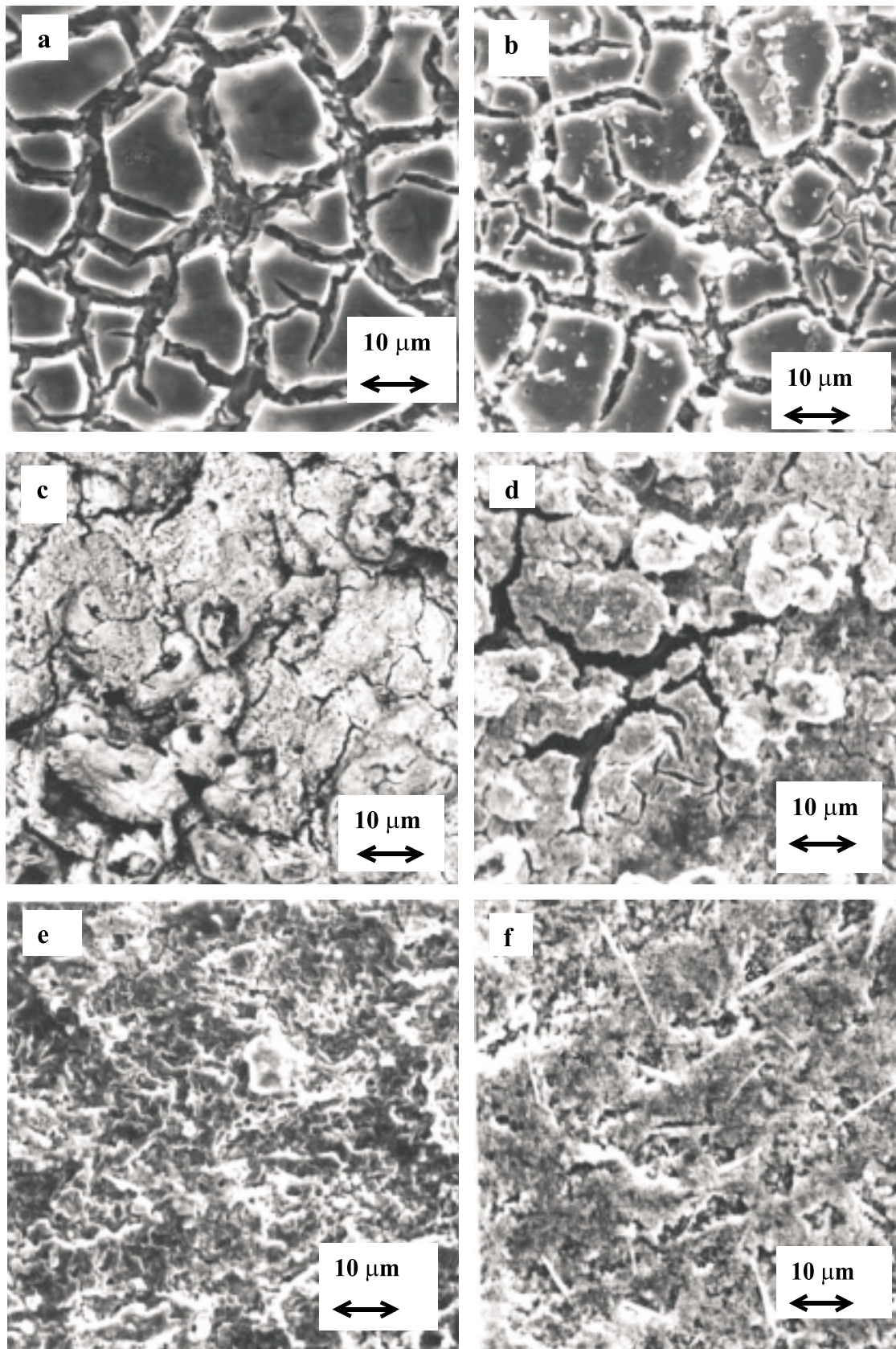


Figure 2. SEM micrographs of the $\text{Ti}/\text{Ir}_{0.3}\text{Ti}_{(0.7-x)}\text{Pb}_x\text{O}_2$ -coated electrodes: (a) freshly-coated $\text{Ti}/\text{Ir}_{0.3}\text{Ti}_{0.7}\text{O}_2$ electrode, (b) $\text{Ti}/\text{Ir}_{0.3}\text{Ti}_{0.7}\text{O}_2$ -coated electrode after Tafel experiment, (c) freshly-coated $\text{Ti}/\text{Ir}_{0.3}\text{Ti}_{0.4}\text{Pb}_{0.3}\text{O}_2$ electrode, (d) $\text{Ti}/\text{Ir}_{0.3}\text{Ti}_{0.4}\text{Pb}_{0.3}\text{O}_2$ -coated electrode after Tafel experiment (e) freshly-coated $\text{Ti}/\text{Ir}_{0.3}\text{Pb}_{0.7}\text{O}_2$ electrode, and (f) $\text{Ti}/\text{Ir}_{0.3}\text{Pb}_{0.7}\text{O}_2$ -coated electrode after Tafel experiment

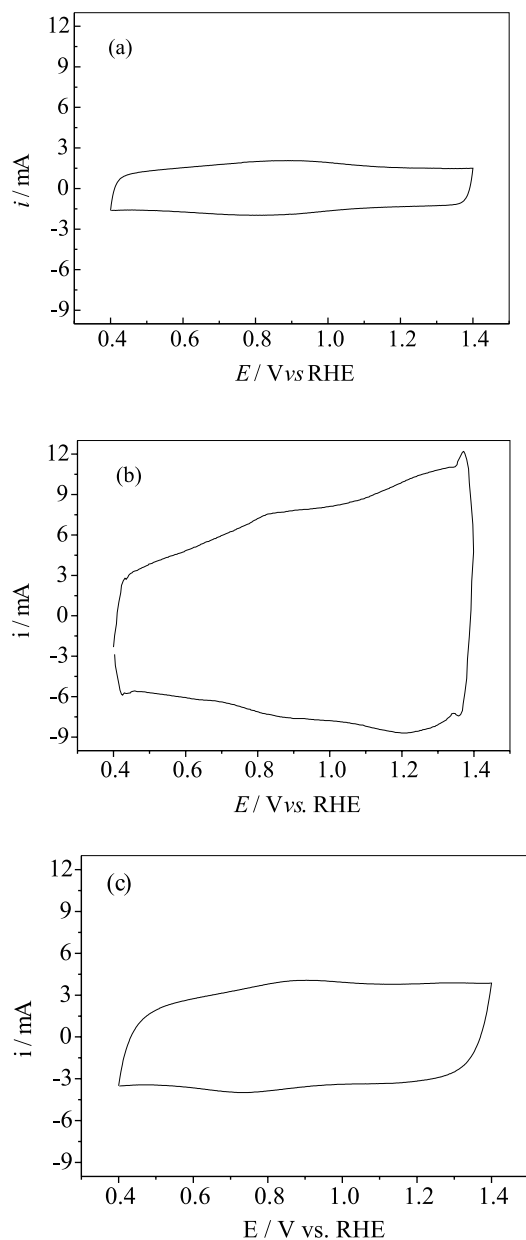


Figure 3. Cyclic voltammograms for the $\text{Ti}/\text{Ir}_{0.3}\text{Ti}_{(0.7-x)}\text{Pb}_x\text{O}_2$ -coated electrodes, heat-treated at $600\text{ }^\circ\text{C}$ for 1 h, in $0.5\text{ mol dm}^{-3}\text{ H}_2\text{SO}_4$ at a scan rate of 20 mV s^{-1} and at room temperature: (a) $\text{Ti}/\text{Ir}_{0.3}\text{Ti}_{0.7}\text{O}_2$ -coated electrode, (b) $\text{Ti}/\text{Ir}_{0.3}\text{Ti}_{0.4}\text{Pb}_{0.3}\text{O}_2$ -coated electrode, and (c) $\text{Ti}/\text{Ir}_{0.3}\text{Pb}_{0.7}\text{O}_2$ -coated electrode

with the lead content and reaches a maximum at 50% PbO_2 . A maximum of q_a with composition is also reported for $\text{Ti}/\text{Ru}_{0.3}\text{Ti}_{(0.7-x)}\text{Sn}_x\text{O}_2$ -coated,¹¹ for $\text{Ti}/\text{Ir}_{0.3}\text{Ti}_{(0.7-x)}\text{Ce}_x\text{O}_2$ -coated¹² and for $\text{Ti}/\text{Ru}_{0.3}\text{Ti}_{(0.7-x)}\text{Ce}_x\text{O}_2$ -coated¹⁴ electrodes. It is related to the deposition of the oxide as a very fine crystallite structure during the thermal decomposition of the precursors, due to the non-intimate mixing between the individual components.¹¹⁻¹⁴ Figure 4 also shows that, after extensive oxygen evolution (Tafel experiments), the

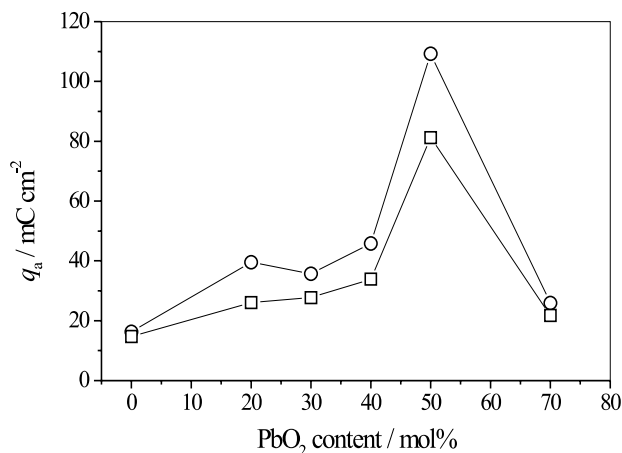


Figure 4. Dependence of the anodic voltammetric charge density with composition for (□) fresh electrodes and (○) for electrodes submitted to Tafel experiments

values of q_a slightly increase. This behavior is explained by Boodts and collaborators¹¹⁻¹⁶ as a result of an increase of the degree coverage of the electrode surface by the active species OH, resulting from water discharge, leading to additional activation of the surface sites.

The OER on the $\text{Ir}_{0.3}\text{Ti}_{(0.7-x)}\text{Pb}_x\text{O}_2$ surfaces was studied by potentiostatic polarisation curves under quasi-steady-state conditions. For all the electrodes, the Tafel lines shows a linear part at potential values less than 1.55 V (E vs. RHE), followed by deviation from linearity at higher potential. The deviation can be associated to ohmic components or to a change in the mechanism.²³ Schub and Reznik²³ and Bisang *et al.*²⁴ developed mathematical models to evaluate ohmic errors and the effect of the geometric parameters, respectively, to correct polarization curves for porous oxide electrodes. The analysis of the deviations using the Schub-Reznik method²⁴ revealed that the deviation from linearity is due to uncompensated resistance effects only, indicating that a single electrode mechanism is operating. The ohmic component values derived from the Schub-Reznik method²⁴ was on the order of $0.7\text{ }\Omega$. This value is in excellent agreement with those normally measured in laboratory cells with a Luggin capillary,²⁵ suggesting that the OER is not influenced by the growth of the isolating TiO_2 film at the substrate/oxide layer interface, and it is consistent with a system containing metallic conductive oxides submerged in a $0.5\text{ mol dm}^{-3}\text{ H}_2\text{SO}_4$ supporting electrolyte.

Typical corrected Tafel plots obtained for all the samples are shown in Figure 5. All the electrodes showed a slope of approximately 60 mV decade^{-1} , which is reported as a Tafel slope characteristic for IrO_2 -based electrodes.²³ However, this Tafel slope value is different from that presented in the literature for $\text{IrO}_2\text{-TiO}_2\text{-CeO}_2$ systems,¹²

which is of $30 \text{ mV decade}^{-1}$. Additionally, the fact that the Tafel slope does not depend on PbO_2 content and, consequently, on the morphology, suggests that only Ir sites are active for OER. This analysis also permits concluding that changes in the morphology or in the composition of the electrode due to the dissolution of the layer during OER do not affect the mechanism of the reaction. This figure also shows that the partial substitution of TiO_2 by PbO_2 ($\text{Ti}/\text{Ir}_{0.3}\text{Ti}_{0.4}\text{Pb}_{0.3}\text{O}_2$) produces an electrocatalyst layer with higher overpotential for the oxygen evolution reaction.

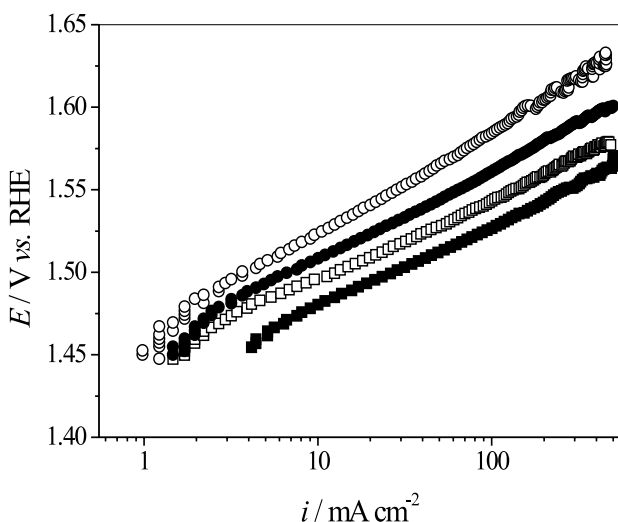


Figure 5. Tafel plots for OER in $0.5 \text{ mol dm}^{-3} \text{ H}_2\text{SO}_4$ at room temperature obtained for $\text{Ti}/\text{Ir}_{0.3}\text{Ti}_{(0.7-x)}\text{Pb}_x\text{O}_2$ -coated electrodes heat-treated at 600°C for 1 h: (\square) $\text{Ti}/\text{Ir}_{0.3}\text{Ti}_{0.7}\text{O}_2$ -coated electrode, (\circ) $\text{Ti}/\text{Ir}_{0.3}\text{Ti}_{0.4}\text{Pb}_{0.3}\text{O}_2$ -coated electrodes, (\blacksquare) $\text{Ti}/\text{Ir}_{0.3}\text{Ti}_{0.2}\text{Pb}_{0.5}\text{O}_2$ -coated electrode and (\bullet) $\text{Ti}/\text{Ir}_{0.3}\text{Pb}_{0.7}\text{O}_2$ -coated electrode

To evaluate the electrocatalytic activity, which can be understood in terms of the S-OH bond strength with PbO_2 content²⁶ (S is a surface active site), the values of current at 1.5 V (E vs RHE) were normalized by the corresponding anodic charge (q_a), and the results are shown in Figure 6. This Figure shows that replacement of the stabilizing oxide (TiO_2) by PbO_2 decreases the electrocatalytic activity of the layers. The normalized current initially decreases with PbO_2 content, reaching a minimum value at 30% PbO_2 , and increases for higher PbO_2 content, with the values of normalized current being approximately constant. The decreasing values of the normalized current can be attributed to a strong S-OH bond, and vice-versa. Decreasing normalized current values at an applied potential were also presented for the $\text{Ti}/\text{Ir}_{0.3}\text{Ti}_{(0.7-x)}\text{Ce}_x\text{O}_2$ -coated electrodes¹² and increasing values for $\text{Ti}/\text{Ru}_{0.3}\text{Ti}_{(0.7-x)}\text{Ce}_x\text{O}_2$ in $1 \text{ mol dm}^{-3} \text{ HClO}_4$.

These results (Figure 5 and 6) suggest that PbO_2 can be a good choice with potential to improve the selectivity of

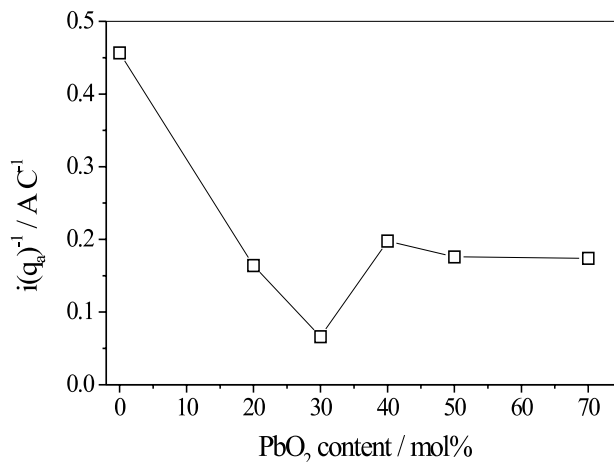


Figure 6. Dependence of the i/q_a with oxide composition for O_2 evolution on $\text{Ti}/\text{Ir}_{0.3}\text{Ti}_{(0.7-x)}\text{Pb}_x\text{O}_2$ -coated electrodes from a $0.5 \text{ mol dm}^{-3} \text{ H}_2\text{SO}_4$ solution. $E = 1.50 \text{ V}$ vs. RHE

the system towards, e.g. chlorine evolution and electrochemical degradation of organic contaminants.

Figure 7 shows the dependence of the rate of the oxygen evolution reaction on the solution pH at constant ionic strength. This figure shows that, within experimental error, the current is constant with the pH. Therefore, $\delta \log i / \text{pH} = 0$. As pointed by Boodts and collaborators,¹¹⁻¹⁶ the observed reaction order is that at constant overpotential [$\nu(\text{H}^+)_{\eta}$] and not at constant potential [$\nu(\text{H}^+)_{\text{E}}$], since the reference electrode used was the hydrogen electrode in the same solution. The chemically significant reaction order is $\nu(\text{H}^+)_{\text{E}}$ which is related to $\nu(\text{H}^+)_{\eta}$ by the equation:

$$\nu(\text{H}^+)_{\text{E}} = \nu(\text{H}^+)_{\eta} - \gamma \quad (1)$$

where γ is the operational transfer coefficient in the Tafel slope ($\delta \log i / \delta h = 2,303RT/\gamma F$). With a value of 60 mV

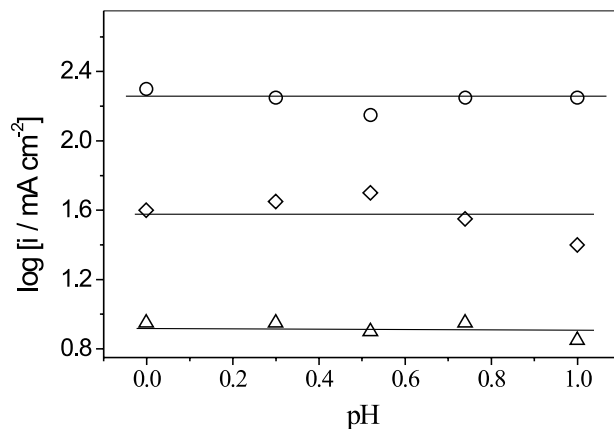


Figure 7. Dependence of the current density at 1.5 V vs. RHE on pH for O_2 evolution on $\text{Ti}/\text{Ir}_{0.3}\text{Ti}_{(0.7-x)}\text{Pb}_x\text{O}_2$ -coated electrodes, heat-treated at 600°C for 1 h at constant ionic strength using a solution containing $c \text{ mol dm}^{-3}$ of H_2SO_4 + $c' \text{ mol dm}^{-3}$ of Na_2SO_4 ($c + c' = 1$): (Δ) $x = 0$; (\diamond) $x = 0.5$; (\circ) $x = 0.7$

decade⁻¹ for the experimental Tafel slope, -1 is obtained for $\nu(\text{H}^+)_{\text{E}}$.

The reaction mechanism is invariant with overpotential and oxide composition, as shown by the Tafel slope and the reaction order. Trasatti and collaborators¹⁴ suggested that the value of 60 mV decade⁻¹ for a Tafel slope is related to the formation of intermediate S-OH as an unstable species, which rearranges via a surface reaction (spillover). The step reaction and Tafel slope for the mechanism is shown in Table 1.

Table 1. Trasatti Mechanism for the Oxygen Evolution Reaction in Acid Media²⁶

| Reaction Step ^a | Tafel Slope / mV decade ⁻¹ |
|---|---------------------------------------|
| (a) $\text{S} + \text{H}_2\text{O} \rightarrow \text{S-OH}^* + \text{H}^+ + \text{e}^-$ | 120 |
| (b) $\text{S-OH}^* \rightarrow \text{S-OH}$ | 60 |
| (c) $\text{S-OH} \rightarrow \text{S-O} + \text{H}^+ + \text{e}^-$ | 40 |
| (d) $\text{S-O} + \text{S-O} \rightarrow \text{O}_2 + 2 \text{S}$ | 15 |

^a S is a surface active site

In this mechanism, the asterisk marks different energy states. If step (b) in the mechanism above is the rate determining step (rds), the kinetics of the reaction is expressed by:^{27,28}

$$i \propto [\text{S-OH}^*] \quad (2)$$

The surface concentration of S-OH* species can be obtained from step (a), regarded as in equilibrium, where the concentration of H₂O and surface sites are independent of the potential:

$$E = \text{constant} + \frac{RT}{F} \ln[\text{S-OH}^*][\text{H}^+] \quad (3)$$

$$[\text{S-OH}^*] = [\text{H}^+]^{-1} \exp[(E - \text{constant})F/RT] \quad (4)$$

The substitution of (4) in equation (1) yields:

$$i \propto [\text{H}^+]^{-1} \exp[(E - \text{constant})F/RT] \quad (5)$$

in agreement with the observed Tafel slope of 60 mV decade⁻¹ and the experimental reaction order of -1.

Conclusions

The thermal method was successfully employed to produce Ti/Ir_{0.3}Ti_(0.7-x)Pb_xO₂-coated electrodes which presented a crystalline structure. The surface morphology of the Ti/Ir_{0.3}Ti_(0.7-x)Pb_xO₂-coated electrodes was influenced

by the composition, being cracked-mud for an IrO₂-TiO₂ layer, showing microcracks for ternary coatings and granular and compact for an IrO₂-PbO₂ layer. The SEM micrographs of the samples used under extensive oxygen evolution (Tafel experiment) suggested that oxygen evolution promotes the dissolution of the layers.

The surface electrochemistry of the electrodes is controlled by the Ir³⁺/Ir⁴⁺ couple. The replacement of TiO₂ by PbO₂ increases the surface area with the highest value being at 50 mol% PbO₂. After extensive use under oxygen evolution conditions the surface area increases slightly. The value of 60 mV decade⁻¹, independent of oxide composition and overpotential, suggests that only Ir sites are active for OER. The values of normalized current show some inhibition of the OER as TiO₂ is replaced by PbO₂, suggesting that PbO₂ can be a good choice with potential to improve the selectivity of the system. The values of Tafel slope and reaction order indicate that a single reaction mechanism is operating.

Acknowledgements

The authors thank the Conselho Nacional de Desenvolvimento Científico e Tecnológico (CNPq) and the Fundação Cearense de Amparo à Pesquisa (FUNCAP), Brazil, for financial assistance.

References

- Trasatti, S.; Lodi, G.; In *Electrodes of Conductive Metallic Oxides*; Trasatti, S., ed.; Elsevier Scientific Publishing Company: Amsterdam, 1981, Part A and B.
- Stucki, S.; Kötzt, R.; Carcer, B.; Suter, W.; *J. Appl. Electrochem.* **1991**, *21*, 99.
- Mráz, R.; Krýsa, J.; *J. Appl. Electrochem.* **1994**, *24*, 1262.
- Ueda, M.; Watanabe, T.; Kameyama, T.; Matsumoto, Y.; Seikimoto, M.; Shimamune, T.; *J. Appl. Electrochem.* **1995**, *25*, 817.
- Correa-Lozano, B.; Comninellis, Ch.; De Battisti, A.; *J. Appl. Electrochem.* **1996**, *26*, 683.
- Lipp, L.; Pletcher, D.; *Electrochim. Acta* **1997**, *42*, 1091.
- Lipp, L.; Pletcher, D.; *Electrochim. Acta* **1997**, *42*, 1101.
- Yang, C. H.; Wen, T. C.; *J. Electrochem. Soc.* **1994**, *141*, 2624.
- Kulandaisamy, S.; Prabhakar, J. R.; Rethinaraj, J.; Choockalingam, C.; Visvanathan, S.; Venkateswaran, K. V.; Ramachandran, P.; Nandakumar, V.; *J. Appl. Electrochem.* **1995**, *27*, 579.
- Kötzt, R.; Stucki, S.; *Electrochim. Acta* **1986**, *31*, 1311.
- Boodts, J. F. C.; Trasatti, S.; *J. Electrochem. Soc.* **1990**, *137*, 3784.

12. Alves, V. A.; da Silva, L. A.; Boodts, J. F. C.; Trasatti, S.; *Electrochim. Acta* **1994**, *39*, 1585.
13. Lassali, T. A. F.; Boodts, J. F. C.; de Castro, S. C.; Landers, R.; Trasatti, S.; *Electrochim. Acta* **1994**, *39*, 1994.
14. de Faria, L. A.; Boodts, J. F. C.; Trasatti, S.; *J. Appl. Electrochem.* **1996**, *26*, 1195.
15. da Silva, L. A.; Alves, V. A.; da Silva, M. A. P.; Trasatti, S.; Boodts, J. F. C.; *Electrochim. Acta* **1996**, *41*, 1279.
16. Lassali, T. A. F.; Bulhões, L. O. S.; Abeid, L. M. C.; Boodts, J. F. C.; *J. Electrochem. Soc.* **1997**, *144*, 3348.
17. Johnson, D. C.; Chang, H.; Feng, J.; Wang, W. In *Electrochemistry for a Cleaner Environment*; Genders, J. D.; Wienberg, N. L., eds.; Electroynthesis Company Incorporated: New York, 1992, p. 331.
18. Mayr, M.; Blatt, W.; Busse, B.; Heinke, H. In *Electrochemistry for a Cleaner Environment*, Genders, J. D.; Wienberg, N. L., eds.; Electroynthesis Company Incorporated: New York, 1992, p. 366.
19. de Souza, C. E.; Machado, S. A. S.; *Quim. Nova* **1993**, *16*, 426.
20. Laurindo, E. A.; Bocchi, N.; Rocha-Filho, R. C.; *J. Braz. Chem. Soc.* **2000**, *11*, 429.
21. Matos-Costa, F. I.; de Lima-Neto, P.; Machado, S. A. S.; Avaca, L. A.; *Electrochim. Acta* **1998**, *44*, 1515.
22. de Oliveira-Sousa, A.; Machado, S. A. S.; Avaca, L. A.; de Lima-Neto, P.; *Electrochim. Acta* **2000**, *45*, 4467.
23. Schub, D. M.; Reznik, M. F.; *Elektrokhimiya* **1985**, *21*, 855.
24. Bisang, J. M.; Jütner, K.; Kreysa, G.; *Electrochim. Acta* **1994**, *39*, 1297.
25. Trasatti, S.; *Electrochim. Acta* **1991**, *36*, 225.
26. Trasatti, S.; *J. Electroanal. Chem.* **1980**, *111*, 125.
27. de Faria, L. A.; *Ph.D. Thesis*, Universidade de São Paulo, Brazil, 1993.
28. da Silva, L. A.; *Ph.D. Thesis*, Universidade de São Paulo, Brazil, 1995.

Received: February 13, 2001

Published on the web: February 25, 2002